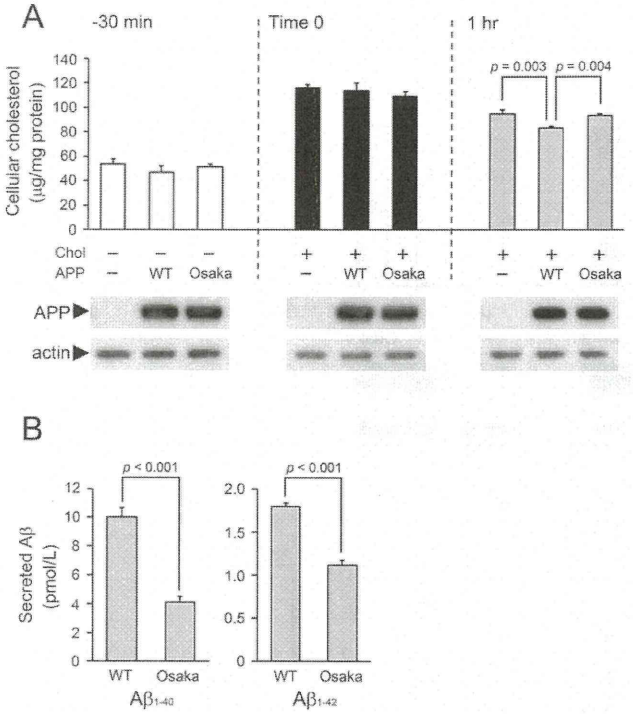

Fig. 2. Impaired Aβ secretion and sustained cellular cholesterol levels in APP_{OSK}-transfected Neuro-2a cells. Neuro-2a cells were transfected with an APP_{WT} or APP_{OSK} construct and loaded with cholesterol. **A:** Cellular cholesterol levels increased significantly immediately after cholesterol loading (solid columns) compared with unloaded cells (open columns). After a 1-hr incubation for cholesterol efflux (shaded columns), APP_{WT}-transfected cells exhibited lower levels of cellular cholesterol than mock-transfected cells, whereas APP_{OSK}-transfected cells exhibited levels of cellular cholesterol that were similar to those of mock-transfected cells. Results are presented as mean ± SEM (n = 4–5). **B:** The concentrations of secreted $A\beta_{40}$ and $A\beta_{42}$ in cultured media were lower in APP_{OSK}-transfected cells than in APP_{WT}-transfected cells. Results are presented as mean ± SEM (n = 5).

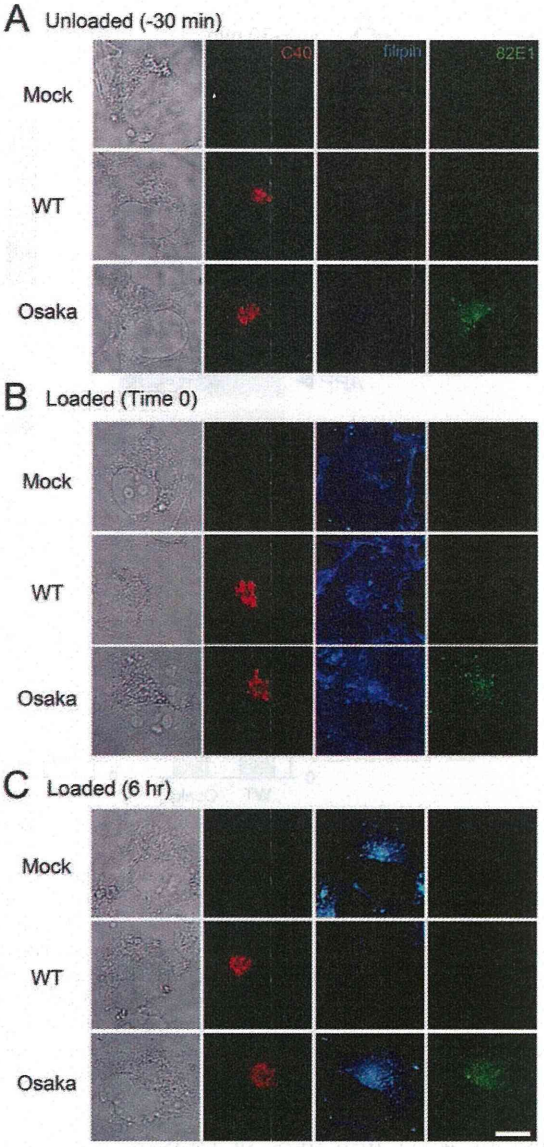

Fig. 3. Intracellular accumulation of Aβ and cholesterol in APP_{OSK}-expressing cells. COS-7 cells were transfected with an APP_{WT} or APP_{OSK} construct and loaded with cholesterol. Intracellular cholesterol and Aβ were visualized with filipin (blue) and an antibody to Aβ (82E1, green). **A:** APP expression was confirmed with an antibody to APP (C40, red) in both APP_{WT}- and APP_{OSK}-transfected cells, but apparent intracellular accumulation of Aβ was observed only in APP_{OSK}-expressing cells. **B:** Increased filipin staining was observed around the plasma membrane immediately after cholesterol loading. **C:** After a 6-hr incubation with cholesterol-free medium, filipin-positive materials were largely sequestered within intracellular compartments. Note that APP_{WT}-expressing cells exhibited only weak filipin staining compared with mock- and APP_{OSK}-expressing cells. Scale bar = 10 μm.

excreted from the cell. To investigate the effect of the Osaka mutation on intracellular cholesterol transport, we examined the subcellular localization of cholesterol and Aβ in APP_{OSK}-expressing cells. The cells were loaded with cholesterol and stained with filipin and 82E1 antibody in combination with a tracker for endosomes/lysosomes (lysotracker) and rabbit antibodies to the ER (anticalnexin) and Golgi apparatus (anti-RCAS1) after a 6-hr incubation. As shown in Figure 4, cholesterol and Aβ accumulated in the endosomes/lysosomes (Fig. 4A), ER (Fig. 4B), and Golgi apparatus (Fig. 4C) in various ratios. We calculated the ratios of filipin intensity of each organelle when whole-cell filipin intensity was assumed to be 100 (Fig. 4D). Approximately 63.0% of cellular cholesterol accumulated in these organelles, with a dominant localization at the ER (38.8%) and a lesser localization at the Golgi apparatus (14.1%) and endosomes/lysosomes (10.1%). The ratios of Aβ intensity of each organelle when whole-cell Aβ intensity was assumed to be 100 were also calculated (Fig. 4E). About 68.4% of cellular Aβ accumulated in these organelles, with a subcellular localization similar to that of cholesterol, except

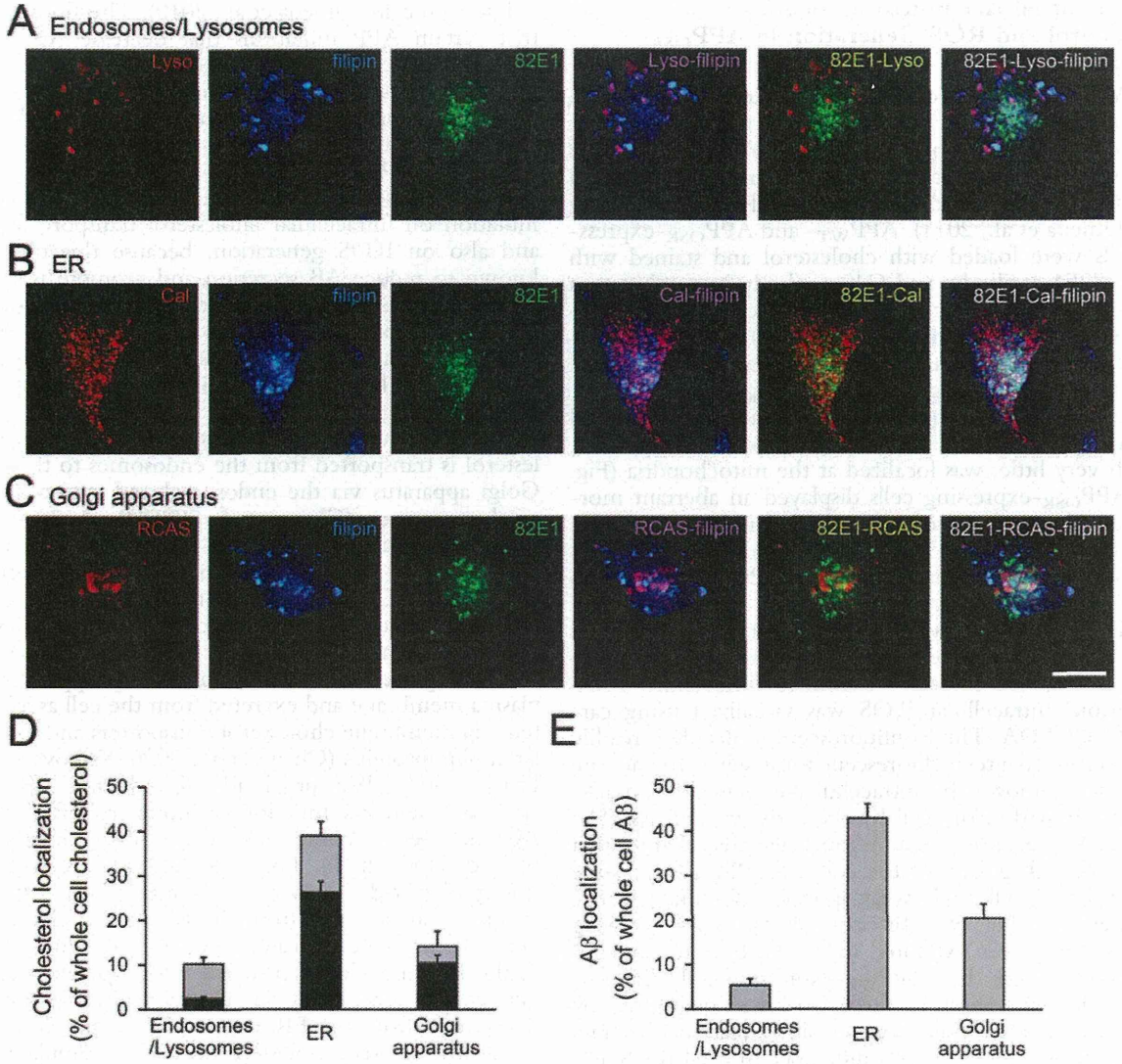

Fig. 4. Subcellular localization of Aβ and cholesterol in APP_{OSK}-expressing cells. COS-7 cells transfected with an APP_{OSK} construct were loaded with cholesterol. Intracellular cholesterol and Aβ were visualized with filipin (blue) and 82E1 antibody (green). The endosomes/lysosomes, ER, and Golgi apparatus were stained with lysotracker (**A**, red), anticalnexin antibody (**B**, red), and anti-RCAS1 antibody (**C**, red), respectively. **D:** The ratios of filipin intensity of each organelle when whole-cell filipin intensity was assumed to be 100 were calculated. The blackened part of each column represents the ratio of cholesterol colocalized with Aβ in the organelle. Results are presented as mean ± SEM (n = 4 for the endosomes/lysosomes, n = 7 for the ER, and n = 6 for the Golgi apparatus). **E:** The ratios of 82E1 intensity of each organelle when whole-cell 82E1 intensity was assumed to be 100 were calculated in the same cells as in D. Cholesterol accumulated predominantly in the ER and to a lesser extent in the Golgi apparatus and endosomes/lysosomes. Aβ showed a subcellular localization similar to that of cholesterol, but far less accumulated in the endosomes/lysosomes. Scale bar = 10 μm.

that Aβ showed far less localization at the endosomes/lysosomes (i.e., ER 42.8%, Golgi apparatus 20.3%, endosomes/lysosomes 5.3%). We further analyzed the ratios of cholesterol colocalized with Aβ in each organelle (Fig. 4D, solid column). About 62.1% of cholesterol accumulated in these organelles was colocalized with Aβ, with a higher colocalization of cholesterol and Aβ at the ER (68.0%) and Golgi apparatus (73.8%) and a lower colocalization at the endosomes/lysosomes (22.8%). These results indicate that, in APP_{OSK}-expressing cells, not only Aβ trafficking from the ER to the plasma membrane but also cholesterol transport from the endosomes to the plasma membrane via the ER and Golgi apparatus were markedly disturbed, suggesting that cholesterol transport from the ER to the plasma membrane depends largely on Aβ trafficking.

Mitochondrial Accumulation of Aβ and Cholesterol and ROS Generation in APP_{OSK}-Expressing Cells

We also examined the mitochondrial accumulation of cholesterol and Aβ, because we previously found that Aβ accumulated not only in the ER, Golgi apparatus, and ensosomes/lysosomes but also in the mitochondria and caused mitochondrial dysfunction in APP_{OSK}-expressing cells (Umeda et al., 2011). APP_{WT}- and APP_{OSK}-expressing cells were loaded with cholesterol and stained with filipin, 82E1 antibody, and C40 antibody in combination with a tracker for mitochondria (Mitotracker). In APP_{WT}-expressing (C40-positive) cells, a few filipin-positive punctae were observed and almost no localization of cholesterol at the mitochondria (Fig. 5A). In APP_{OSK}-expressing cells, on the other hand, abundant accumulation of cholesterol and Aβ was observed, and a portion of these materials, though very little, was localized at the mitochondria (Fig. 5B). APP_{OSK}-expressing cells displayed an aberrant morphology of mitochondrial networks and reduced and fragmented staining with mitotracker, which is consistent with our previous report (Umeda et al., 2011) and suggests severe mitochondrial dysfunction.

It has been shown that mitochondrial cholesterol exacerbates Aβ-induced ROS generation (Fernandez et al., 2009). We therefore examined intracellular ROS generation. Intracellular ROS was visualized using carboxy H_2DCFDA. This nonfluorescent molecule is readily converted to its green-fluorescent form when the acetate groups are removed by intracellular esterases and oxidation occurs within the cell by the activity of ROS. The converted form possesses additional negative charges that impede its leakage out of the cell. In APP_{WT}-expressing (C40-positive) cells, only weak spots of DCF fluorescence were detected (Fig. 5C). In contrast, APP_{OSK}-expressing (C40-positive) cells exhibited more and brighter spots of DCF fluorescence than APP_{WT}-expressing cells did (Fig. 5D). ROS generation in these cells was quantified by measuring the DCF fluorescence using a plate reader (Fig. 5E). There was no significant difference in basal ROS levels in the absence of cholesterol loading between mock-, APP_{WT}-, and APP_{OSK}-transfected cells, although there was a tendency for intracellular ROS generation to increase in the following ascending order: mock-transfected cells, APP_{WT}-transfected cells, and APP_{OSK}-transfected cells. Cholesterol loading considerably increased ROS levels in all cell types, although the effect was much greater in APP_{OSK}-transfected cells than in mock- or APP_{WT}-transfected cells. This is probably because both the Aβ-induced ROS generation and cholesterol that depleted mitochondrial glutathione had accumulated most in the APP_{OSK}-expressing cells.

DISCUSSION

We have previously shown that cellular cholesterol levels are regulated by Aβ secretion. During its secretion, Aβ assembles high-density lipoprotein (HDL)-like complexes with cellular cholesterol via ABCA1, leading to cholesterol efflux from cells (Umeda et al., 2010). This finding implies that certain APP mutations that decrease Aβ secretion may also disturb Aβ-mediated cholesterol efflux and induce cholesterol accumulation within a cell. Furthermore, such abnormal accumulation of cellular cholesterol may elicit cellular malfunction such as an enhancement of Aβ-induced ROS generation (Fernandez et al., 2009). Thus, the present study examined the effect of the Osaka mutation on intracellular cholesterol transport and efflux and also on ROS generation, because this mutation is known to reduce Aβ secretion and promote intracellular Aβ accumulation (Tomiyama et al., 2008; Nishitsuji et al., 2009). As expected, we found that the Osaka mutation caused an intracellular accumulation of cholesterol and Aβ and enhanced ROS generation in cultured cells upon cholesterol loading.

It is known that, after being taken up by cells, cholesterol is transported from the endosomes to the ER and Golgi apparatus via the endosomal and cytosolic cholesterol transporters (Chang et al., 2006; Prinz, 2007; Subramanian and Balch, 2008). Cells are thought to have some kind of sensor such as acyl-coenzyme A:cholesterol acyltransferase (ACAT) in the ER that can monitor intracellular cholesterol levels and accordingly regulate de novo cholesterol synthesis (Chang et al., 2006). Cholesterol is then transported from the ER and Golgi apparatus to the plasma membrane and excreted from the cell as a lipoprotein via membrane cholesterol transporters and extracellular apolipoproteins (Chang et al., 2006; Yokoyama, 2006; Prinz, 2007). We previously found that Aβ has an apolipoprotein-like function in cholesterol efflux and that Aβ/cholesterol complexes may form intracellularly (Umeda et al., 2010). This latter finding suggests the possibility that Aβ is involved in intracellular cholesterol transport, such as that from the ER to the plasma membrane. If this were the case, cholesterol would accumulate in the ER and Golgi apparatus with Aβ when Aβ trafficking is disturbed. On the contrary, if cholesterol were transported from the ER to the plasma membrane independently of Aβ, cholesterol would accumulate in the plasma membrane without any Aβ colocalization. Here, we showed that, in APP_{OSK}-expressing cells, cholesterol accumulated in the ER, Golgi apparatus, and endosomes/lysosomes, whereas intracellular Aβ accumulated predominantly in the ER and Golgi apparatus only, the intra-ER accumulation being more prominent than the intra-Golgi accumulation. These results imply that the disturbed trafficking of Aβ from the ER to the plasma membrane affects cholesterol transport to cause cholesterol accumulation within the ER and Golgi apparatus. The observed cholesterol accumulation within the endosomes/lysosomes could be the result of a cellular response that prevents further influx of cholesterol from the endosomes to the ER. In APP_{WT}-expressing cells, Aβ trafficking is undisturbed, so cholesterol was transported from the ER to the plasma membrane and discharged from the cell (Figs. 1–3). These findings appear to support the idea that Aβ is involved in cholesterol transport from the ER to the plasma membrane as well as cholesterol efflux from

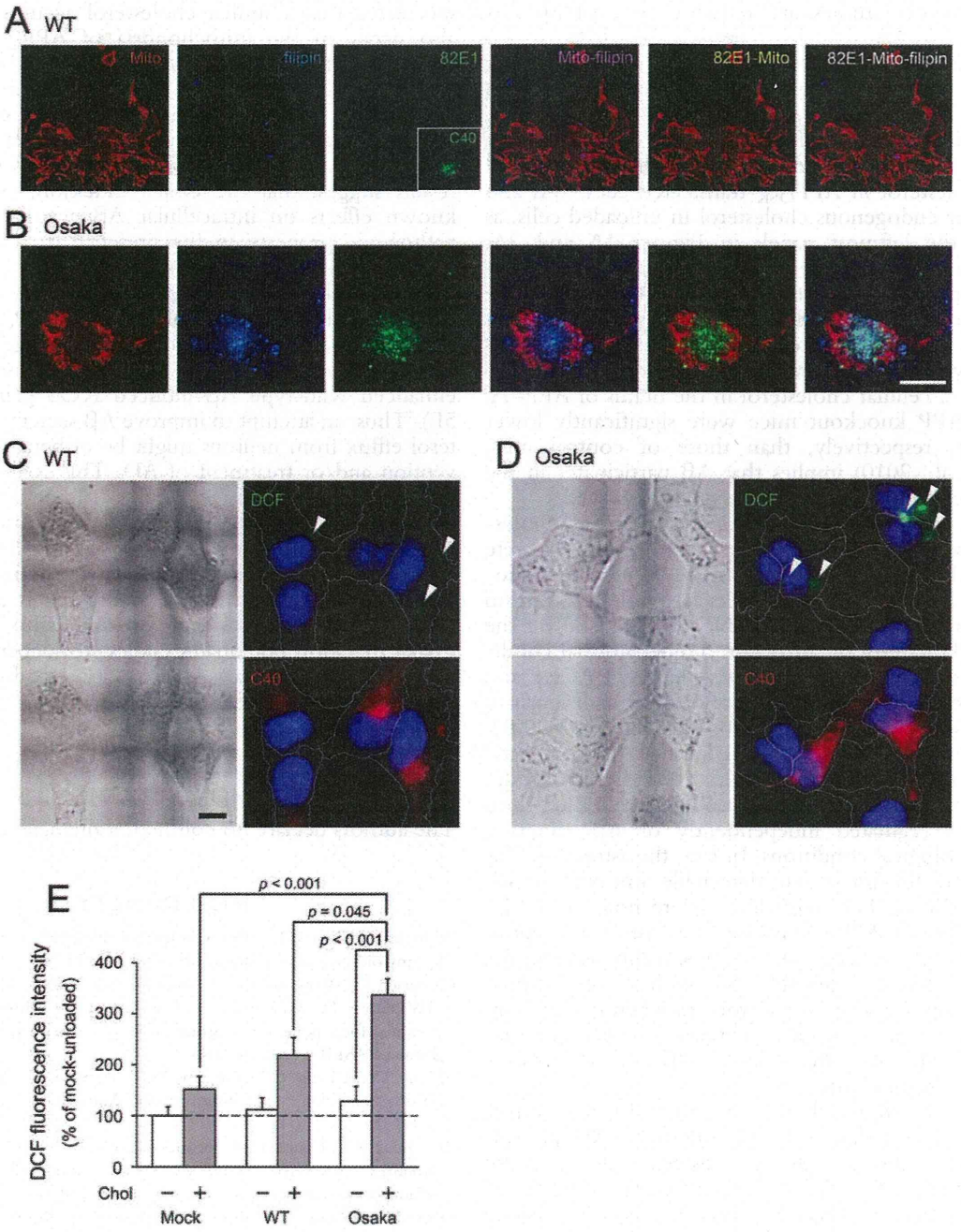

Fig. 5. Mitochondrial accumulation of Aβ and cholesterol and ROS generation in APP_{OSK}-expressing cells. COS-7 cells were transfected with an APP_{WT} (A,C) or APP_{OSK} (B,D) construct and loaded with cholesterol. Mitochondrial localization of cholesterol and Aβ was examined with filipin (blue), 82E1 antibody (green), and mitotracker (red). APP expression was confirmed with C40 antibody (A **inset**, green). **A:** In APP_{WT}-expressing cells, only a few filipin-positive punctae were observed and almost no localization of cholesterol at the mitochondria. **B:** In APP_{OSK}-expressing cells, a portion of cholesterol and Aβ accumulated in the mitochondria, and these materials were partially colocalized. **C,D:** For the visualization of intracellular ROS, cells were stained with carboxy H_2DCFDA, followed by counterstaining with Hoechst 33342. Phase-contrast images and DCF fluorescence (green, arrowheads) were taken before cell fixation (upper rows in C,D). The cells were then fixed and stained with C40 antibody to confirm APP expression (red, lower rows). **E:** Intracellular ROS was quantified by measuring DCF fluorescence with a multiplate reader. Cholesterol loading considerably increased ROS levels in all cells. The increased ROS generation induced by cholesterol loading was much greater in APP_{OSK}-transfected cells than in mock- and APP_{WT}-transfected cells. Results are presented as mean ± SEM (n = 8). Scale bar = 10 micrometer in B (applies to A, B) and C (applies to C, D).

the cell. Further studies are required to establish this conclusion.

The effect of the Osaka mutation on intracellular cholesterol transport and efflux was clearly demonstrated here in cultured cells after exogenous cholesterol loading. The same tendency, i.e., lower levels of cellular cholesterol in APP_{WT}-transfected cells and unchanged levels of cellular cholesterol in APP_{OSK}-transfected cells, was also observed for endogenous cholesterol in unloaded cells, as shown in the leftmost panels in Figures 1A and 2A, although the changes were relatively mild. It may be that Aβ functions in particular to correct an abnormal increase of cellular cholesterol levels, so its effect was not so evident when cellular cholesterol levels were in the normal range. However, our previous observation that steady-state levels of cellular cholesterol in the brains of APP-Tg mice and APP knockout mice were significantly lower and higher, respectively, than those of control mice (Umeda et al., 2010) implies that Aβ participates in the regulation of endogenous cholesterol levels as well.

In the brain, astrocytes play a critical role in cholesterol turnover (Pfrieger and Ungerer, 2011). They secrete HDL-type lipoproteins to deliver newly synthesized cholesterols to neurons and collect extra cholesterols from neurons for their redistribution. Neurons depend on the supply of cholesterol by astrocytes. Under normal conditions, astrocytes express very low levels of BACE1 and thus produce very little Aβ in spite of their high levels of APP expression (Zhao et al., 1996; Rossner et al., 2001); astrocytes come to express BACE1 when they are activated (Hartlage-Rübsamen et al., 2003; Hong et al., 2003). These findings suggest that cholesterol efflux from astrocytes is regulated independently of Aβ secretion under physiological conditions. In fact, the astrocytic cells that we used did not secrete detectable amounts of Aβ, and their cellular choresterol levels were not affected by the expression of APP. In resting-state astrocytes, apoE, ABCA1, and other factors, if any, presumably mediate the cholesterol efflux. It is possible that Aβ has a role to promote cholesterol efflux from astrocytes when the cells are activated under pathological conditions. The Osaka mutation in astrocytes may affect such an Aβ-induced promotion of cholesterol efflux.

It has been shown that the mitochondria are a direct site for Aβ accumulation in neurons from AD patients and transgenic mouse models (Caspersen et al., 2005; Manczak et al., 2006). Aβ is thought to access the mitochondrial matrix via intracellular trafficking and mediate mitochondrial toxicity, including metabolic enzyme defects, respiratory chain dysfunction, and ROS generation (Caspersen et al., 2005; Manczak et al., 2006). We have demonstrated that Aβ that accumulated in the mitochondria causes mitochondrial dysfunction and subsequent cell death in APP_{OSK}-transfected cells and the brains of APP_{OSK}-Tg mice (Umeda et al., 2011). Another study has shown that mitochondrial cholesterol increases the susceptibility of neurons to $A\beta_{42}$-induced oxidative stress, probably by a cholesterol-mediated depletion of mitochondrial glutathione (Fernandez et al., 2009). We speculated that a similar cholesterol accumulation might also occur in the mitochondria of APP_{OSK}-expressing cells upon cholesterol loading, which would enhance Aβ-induced ROS generation. Supporting this theory, we detected an increase in the accumulation of cholesterol and Aβ in the mitochondria of APP_{OSK}-expressing cells and an accompanying increase in ROS generation. These results suggest that the Osaka mutation, along with its known effects on intracellular Aβ accumulation, has a pathogenic property in the presence of cholesterol that sensitizes cells to oxidative stress. We have also observed that the Osaka mutation-induced pathology can be accelerated by hypercholesterolemia in APP_{OSK}-Tg mice (Umeda et al., 2012). Evidence here suggests that this might apply to APP_{WT} as well, because cholesterol enhanced wild-type Aβ-induced ROS generation (Fig. 5E). Thus, an attempt to improve Aβ secretion and cholesterol efflux from neurons might be of benefit for the prevention and/or treatment of AD. This could be achieved by stimulation of synaptic activity (Tampellini et al., 2009) by means of learning, exercise, and so on. Antioxidants and cholesterol-lowering medicine would also be effective for attenuating intracellular Aβ toxicity. In summary, the present findings suggest that Aβ trafficking is important for intracellular cholesterol transport and efflux and that the Osaka mutation potentiates cholesterol-dependent exacerbation of intracellular Aβ toxicity by disturbing Aβ-mediated cholesterol efflux from the cell.

ACKNOWLEDGMENTS

The authors declare no conflicting financial interests.

REFERENCES

Bodovitz S, Klein WL. 1996. Cholesterol modulates α-secretase cleavage of amyloid precursor protein. J Biol Chem 271:4436–4440.

Caspersen C, Wang N, Yao J, Sosunov A, Chen X, Lustbader JW, Xu HW, Stern D, McKhann G, Yan SD. 2005. Mitochondrial Aβ: a potential focal point for neuronal metabolic dysfunction in Alzheimer's disease. FASEB J 19:2040–2041.

Chang TY, Chang CC, Ohgami N, Yamauchi Y. 2006. Cholesterol sensing, trafficking, and esterification. Annu Rev Cell Dev Biol 22: 129–157.

Fernandez A, Llacuna L, Fernandez-Checa JC, Colell A. 2009. Mitochondrial cholesterol loading exacerbates amyloid β peptide-induced inflammation and neurotoxicity. J Neurosci 29:6394–6405.

Frears ER, Stephens DJ, Walters CE, Davies H, Austen BM. 1999. The role of cholesterol in the biosynthesis of β-amyloid. Neuroreport 10: 1699–1705.

Hartlage-Rübsamen M, Zeitschel U, Apelt J, Gärtner U, Franke H, Stahl T, Günther A, Schliebs R, Penkowa M, Bigl V, Rossner S. 2003. Astrocytic expression of the Alzheimer's disease β-secretase (BACE1) is stimulus-dependent. Glia 41:169–179.

Hong HS, Hwang EM, Sim HJ, Cho HJ, Boo JH, Oh SS, Kim SU, Mook-Jung I. 2003. Interferon γ stimulates β-secretase expression and sAPPβ production in astrocytes. Biochem Biophys Res Commun 307: 922–927.

Manczak M, Anekonda TS, Henson E, Park BS, Quinn J, Reddy PH. 2006. Mitochondria are a direct site of Aβ accumulation in Alzheimer's

disease neurons: implications for free radical generation and oxidative damage in disease progression. Hum Mol Genet 15:1437–1449.

Nishitsuji K, Tomiyama T, Ishibashi K, Ito K, Teraoka R, Lambert MP, Klein WL, Mori H. 2009. The E693Δ mutation in amyloid precursor protein increases intracellular accumulation of amyloid β oligomers and causes endoplasmic reticulum stress-induced apoptosis in cultured cells. Am J Pathol 174:957–969.

Pfrieger FW, Ungerer N. 2011. Cholesterol metabolism in neurons and astrocytes. Prog Lipid Res 50:357–371.

Prinz WA. 2007. Non-vesicular sterol transport in cells. Prog Lipid Res 46:297–314.

Rossner S, Apelt J, Schliebs R, Perez-Polo JR, Bigl V. 2001. Neuronal and glial β-secretase (BACE) protein expression in transgenic Tg2576 mice with amyloid plaque pathology. J Neurosci Res 64: 437–446.

Solomon A, Kivipelto M. 2009. Cholesterol-modifying strategies for Alzheimer's disease. Expert Rev Neurother 9:695–709.

Stefani M, Liguri G. 2009. Cholesterol in Alzheimer's disease: unresolved questions. Curr Alzheimer Res 6:15–29.

Subramanian K, Balch WE. 2008. NPC1/NPC2 function as a tag team duo to mobilize cholesterol. Proc Natl Acad Sci U S A 105:15223–15224.

Suga K, Tomiyama T, Mori H, Akagawa K. 2004. Syntaxin 5 interacts with presenilin holoproteins, but not with their N- or C-terminal fragments, and affects β-amyloid peptide production. Biochem J 381:619–628.

Tampellini D, Rahman N, Gallo EF, Huang Z, Dumont M, Capetillo-Zarate E, Ma T, Zheng R, Lu B, Nanus DM, Lin MT, Gouras GK. 2009. Synaptic activity reduces intraneuronal Aβ, promotes APP transport to synapses, and protects against Aβ-related synaptic alterations. J Neurosci 29:9704–9713.

Tomiyama T, Nagata T, Shimada H, Teraoka R, Fukushima A, Kanemitsu H, Takuma H, Kuwano R, Imagawa M, Ataka S, Wada Y, Yoshioka E, Nishizaki T, Watanabe Y, Mori H. 2008. A new amyloid β variant favoring oligomerization in Alzheimer's-type dementia. Ann Neurol 63:377–387.

Tomiyama T, Matsuyama S, Iso H, Umeda T, Takuma H, Ohnishi K, Ishibashi K, Teraoka R, Sakama N, Yamashita T, Nishitsuji K, Ito K, Shimada H, Lambert MP, Klein WL, Mori H. 2010. A mouse model of amyloid β oligomers: their contribution to synaptic alteration, abnormal tau phosphorylation, glial activation, and neuronal loss in vivo. J Neurosci 30:4845–4856.

Umeda T, Mori H, Zheng H, Tomiyama T. 2010. Regulation of cholesterol efflux by amyloid β secretion. J Neurosci Res 88:1985–1994.

Umeda T, Tomiyama T, Sakama N, Tanaka S, Lambert MP, Klein WL, Mori H. 2011. Intraneuronal amyloid β oligomers cause cell death via endoplasmic reticulum stress, endosomal/lysosomal leakage, and mitochondrial dysfunction in vivo. J Neurosci Res 89:1031–1042.

Umeda T, Tomiyama T, Kitajima E, Idomoto T, Nomura S, Lambert MP, Klein WL, Mori H. 2012. Hypercholesterolemia accelerates intraneuronal accumulation of Aβ oligomers resulting in memory impairment in Alzheimer's disease model mice. Life Sci 91:1169–1176.

Xiong H, Callaghan D, Jones A, Walker DG, Lue LF, Beach TG, Sue LI, Woulfe J, Xu H, Stanimirovic DB, Zhang W. 2008. Cholesterol retention in Alzheimer's brain is responsible for high β- and γ-secretase activities and Aβ production. Neurobiol Dis 29:422–437.

Yokoyama S. 2006. Assembly of high-density lipoprotein. Arterioscler Thromb Vasc Biol 26:20–27.

Zhao J, Paganini L, Mucke L, Gordon M, Refolo L, Carman M, Sinha S, Oltersdorf T, Lieberburg I, McConlogue L. 1996. β-Secretase processing of the β-amyloid precursor protein in transgenic mice is efficient in neurons but inefficient in astrocytes. J Biol Chem 271:31407–31411.

Journal of Alzheimer's Disease 38 (2014) 601–609
DOI 10.3233/JAD-130632
IOS Press

Protein Disulfide Isomerase P5-Immunopositive Inclusions in Patients with Alzheimer's Disease

Yasuyuki Honjo[a,b,1], Tomohisa Horibe[a,1], Aya Torisawa[a], Hidefumi Ito[c], Aki Nakanishi[d], Hiroshi Mori[e], Tohru Komiya[f], Ryosuke Takahashi[b] and Koji Kawakami[a,*]
[a]*Department of Pharmacoepidemiology, Graduate School of Medicine and Public Health, Kyoto University, Kyoto, Japan*
[b]*Department of Neurology, Graduate School of Medicine, Kyoto University, Kyoto, Japan*
[c]*Department of Neurology, Graduate School of Medicine, Wakayama Medical University, Wakayama, Japan*
[d]*Department of Neurology and Psychiatry, Osaka City Kosaiin Hospital, Osaka, Japan*
[e]*Department of Neurology and Neuroscience, Osaka City University Medical School, Osaka, Japan*
[f]*Faculty of Bioscience, Nagahama Institute of Bioscience and Technology, Shiga, Japan*

Accepted 26 July 2013

Abstract. Amyloid plaques and neurofibrillary tangles (NFTs) are the major pathological characteristics of Alzheimer's disease (AD). NFTs are composed of tubular filaments and paired helical filaments containing polymerized hyperphosphorylated tau protein. Another feature of AD is excessive generation of nitric oxide (NO). Protein disulfide isomerase (PDI) is a chaperon protein located in the endoplasmic reticulum (ER). It was recently reported that NO-induced S-nitrosylation of PDI inhibits its enzymatic activity, leading to the accumulation of polyubiquitinated proteins, and activates the unfolded protein response. In addition, we previously reported the presence of PDI-immunopositive NFTs in AD. Here, we found that protein disulfide isomerase P5 (P5), which is a member of the PDI protein family, was co-localized with tau in NFTs. To our knowledge, this is the first report of P5-immunopositive inclusion in AD. Furthermore, we showed that S-nitrosylated P5 was present and the expression level of P5 was decreased in AD brains compared with that of control brains. We also demonstrated that the knock-down of PDI or P5 by siRNA could affect the viability of SH-SY5Y cells under ER stress. Previously, the observation of S-nitrosylated PDI in AD was reported. NO may inhibit P5 by inducing S-nitrosylation in the same manner as PDI, which inhibits its enzymatic activity allowing protein misfolding to occur in AD. The accumulation of misfolded proteins induces ER stress and may cause apoptosis of neuronal cells through S-nitrosylation and down-regulation of PDI and P5 in AD.

Keywords: Alzheimer's disease, endoplasmic reticulum stress, misfolding, neurofibrillary tangle, nitric oxide, protein disulfide isomerase, protein disulfide isomerase P5, S-nitrosylation, tau

INTRODUCTION

The morphology of Alzheimer's disease (AD) includes cerebral atrophy, deposition of amyloid-β (Aβ; senile plaques), and neuritic changes, including neurofibrillary tangles (NFTs) [1]. Tau, which is normally localized to neurons as a microtubule-associated protein, is abnormally phosphorylated and deposited in NFTs [1]. Furthermore, NFTs are associated with the clinical progressive stage of AD [1]. Ultrastructural studies have shown that NFTs are composed of paired helical filaments containing polymerized hyperphosphorylated tau protein [1, 2]. Tau and Aβ are two major pathological hallmarks of AD.

[1]These authors contributed equally to this work.

*Correspondence to: Koji Kawakami, Department of Pharmacoepidemiology, Graduate School of Medicine and Public Health, Kyoto University, Yoshida Konoecho, Sakyoku, Kyoto 606-8501, Japan. Tel.: +81 75 753 4459; Fax: +81 75 753 4469; E-mail: kawakami.koji.4e@kyoto-u.ac.jp.

Another characteristic of AD is excessive generation of nitric oxide (NO) due to the *N*-methyl-D-aspartate (NMDA) subtype of glutamate receptors. Physiologically, the NMDA receptor mediates post-synaptic Ca^{2+} influx, but excessive influx can cause excitotoxicity [3]. NO can contribute to neuronal cell injury and death in many neurodegenerative diseases [3]. Furthermore, inhibition of NO activity ameliorates the progression of disease pathology in animal models of AD [4]. The accumulation of misfolded, aggregated proteins and Ca^{2+} influx can cause endoplasmic reticulum (ER) stress in neurons. ER stress signaling, otherwise known as the unfolded protein response, is triggered by an increased amount of misfolded proteins in the organelle [3].

Protein disulfide isomerase P5 (P5) is a member of the protein disulfide isomerase (PDI) family, contains both the secretory signal sequence at its N-terminus and the ER retrieval signal (KDEL) at its C-terminus, and is mostly localized in the ER lumen as many other soluble PDI family members [5, 6]. Currently, there are at least 20 identified members of this family, each of which is characterized by the presence of at least one domain that is homologous to thioredoxin. Many of these domains contain a pair of active site cysteine residues (CXXC) that shuttle between the disulphide and dithiol form [7]. To perform disulphide exchange reactions, the individual active sites must be maintained in either the oxidized disulphide form to allow disulphide formation, or the reduced dithiol form for isomerization or reduction of disulphide bonds [5–7]. Although the detailed functions of P5 in the cells remains obscure, it was recently reported that P5 localized not only to the ER but also the mitochondria, and mitochondrial P5 could also suppress oxidative stress-induced cell death [5, 8]. These previous findings suggest that P5 may have significant physiological functions for quality control in both locations [5, 8]. In addition, the observation of S-nitrosylated PDI in AD has been reported [9]. PDI is an ER chaperon protein but the chaperon function is lost when PDI is S-nitrosylated. Furthermore, we have previously reported the presence of PDI-immunopositive NFTs and dystrophic neurites in AD [10].

The ER stress response depends on the stress burden. It is protective and adaptive when the degree of ER stress is moderate. Failure of the adaptive response leads to the activation of an inflammatory response. When the ER stress burden is high and prolonged, executioner pathways are activated. P5 substrate immunoglobulin heavy chain-binding protein (BiP), an ER stress marker that is localized to the ER, prevents neuronal cell death by ER stress. BiP was reported to be increased in the brain of patients with AD, dependent on the clinical stage of disease [11]. Here we report that S-nitrosylated P5 is present and the expression level of P5 is decreased in AD. We also found that the knock-down of PDI or P5 by siRNA could affect the cell viability of SH-SY5Y cells in conditions of ER stress. Furthermore, P5 and tau are co-localized in NFTs of AD brain.

MATERIALS AND METHODS

Materials

Rabbit anti-PDI and anti-P5 antibodies were raised against purified bovine PDI and recombinant human P5 purified from *E. coli*, and anti-P5 antibody was further affinity purified [5, 7, 8]. It was confirmed by western blotting that these antibodies do not cross-react with each other (Supplementary Fig. 1) [5, 7, 8]. Anti-S-nitrosocysteine (anti-SNO-Cys) antibody was purchased from Abcam (Cambridge, UK). Protein G PLUS-Agarose was purchased from Santa Cruz Biotechnology (Santa Cruz, CA, USA). Anti-β-actin antibody was purchased from Sigma (St Louis, MO, USA). Other reagents including thapsigargin were obtained from Nacalai Tesque (Kyoto, Japan). All reagents were of analytical grade. Postmortem brain specimens from 10 patients with AD (67–98 years old) and 8 normal control brains (62–94 years old) were utilized in this study as shown in Table 1. This study was approved by the local ethics committee. Informed consent was obtained from all individuals or their guardians before the analysis. Patient diagnosis was obtained by pathological examination. Specimens from the hippocampus and frontal lobe were obtained from the autopsied brains of the normal control and AD patients. Brains were fixed in 10% neutral formalin at room temperature except for frozen samples. Paraffin-embedded tissue blocks were prepared and cut into 6-μm-thick sections on a microtome. The paraffin-embedded sections were deparaffinized and then rehydrated in ethanol solutions of decreasing concentration as previously described [10, 12].

Immunohistochemistry

Immunohistochemical staining was performed as previously described [10, 12]. Immunohistochemical staining for P5 was performed using polyclonal rabbit anti-P5 antibody as previously described [5, 8]. Briefly,

Table 1
Clinical profiles of all AD patients and controls

Case	Gender	Age (years)	PMI (h)	Cause of death
Control				
1	M	62	3	Pancreatic cancer
2	F	94	NA	Pneumonia
3	M	92	9	Pneumonia
4	M	70	11	Pneumonia
5	M	91	11	Heart failure
6	M	63	NA	Heart failure
7	F	71	4	Lung cancer
8	M	62	NA	Heart failure
Alzheimer's Disease				
1	F	84	4	Heart failure
2	F	89	2.5	Sepsis
3	F	81	11	Pneumonia
4	F	71	11	Pneumonia
5	F	80	11	Heart failure
6	F	98	11	Pneumonia
7	F	93	5	Pneumonia
8	F	94	15	Renal failure
9	M	77	1.5	Pneumonia
10	F	67	18	Leukemia

M, male; F, female, age, age at death, PMI, postmortem interval, NA, not available.

sections were incubated in a microwave oven for a few minutes. After washing with phosphate-buffered saline (PBS) containing 0.3% Triton X100 (PBST), sections were incubated with the primary antibody diluted in PBST overnight at room temperature. After incubation with the primary antibody and washing, sections were incubated with the secondary antibody. The sections were incubated with an avidin–biotin complex, and were allowed to react with a solution containing 0.02% 3,3′-diaminobenzidine tetrahydrochloride (DAB), 0.005% hydrogen peroxide, and 0.6% nickel acetate in 0.0 5 M Tris/HCl buffer.

Double staining of P5 and a marker of NFT in tissue sections from AD samples

To confirm the anatomical relationship between P5 and NFT, we performed double-staining studies using mouse anti-AT8 and rabbit anti-P5 antibodies as described previously [10, 12]. Double staining was performed using mouse anti-AT8 antibody purchased from Innogenetics Biologicals (Ghent, Belgium). Briefly, sections of the hippocampus were incubated in medium containing mouse anti-AT8 and anti-P5 antibodies in PBST overnight at room temperature. After washing, the sections were reacted with secondary antibody for 1 h at room temperature. After rinsing, the slides were mounted with Vectashield (Vector Laboratories, Burlingame, CA, USA) and photographed using an Olympus Fr1000 (Olympus corporation, Tokyo, Japan) confocal laser scanning microscope. A total of 100 AT8-immunopositive NFTs in the immunostained sections of the hippocampus were selected from three patients with AD. The number of P5-immunopositive NFTs in the selected AT8-immunopositive NFTs was then counted from each patient.

Cell culture

The human neuroblastoma cell line SH-SY5Y was purchased from the European Collection of Cell Culture (ECACC, Salisbury, UK). SH-SY5Y cells were cultured in Dulbecco's modified Eagle's medium containing 10% fetal bovine serum, 100 μg/ml penicillin, and 100 μg/ml streptomycin at 37°C in 5% CO_2/95% air.

siRNA transfection

The following Stealth RNAi duplexes (Invitrogen, Carlsbad, CA, USA) were used for knock-down experiments for PDI and P5. PDI: 5′-CAGAGGCCAUCGAUGACAUACCAUU-3′ and 5′-AAUGGUAUGUCAUCGAUGGCCUCUG-3′; P5: 5′-CCAUAUCCUUGAUACUGGAGCUGCA-3′ and 5′-UGCAGCUCCAGUAUCAAGGAUAUGG-3′.

Stealth RNAi-negative control duplex (Invitrogen), with a GC content similar to that of each duplex siRNA, was used as a "scrambled" negative control. siRNA transfection was performed as described previously [8]. Briefly, SH-SY5Y cells were grown to 40–50% confluence on a six-well plate and transfected with the above siRNAs using Lipofectamine RNAiMAX (Invitrogen) according to the manufacturer's instructions.

Cell viability assay

Cell viability was determined by using the WST-8 assay as described previously [13, 14]. Briefly, cells were seeded onto 96-well plates at 5000 cells/well 48 h after transfection. The cell viability assay was carried out after induction of ER stress by 0.5 μM of thapsigargin which was compared with non-thapsigargin assay using Living Cell Count Reagent SF (Nacalai Tesque, Kyoto, Japan) according to the manufacturer's protocol. Absorbance was measured at a wavelength of 450 nm using a 96-well microplate reader (GE Healthcare Bioscience, Little Chalfont, UK). Data represent the mean ± SD from experiments performed in triplicate.

Western blotting

Protein extraction from human brain samples from six patients with AD (71–98 years old) and five control patients (62–94 years old) was performed as described previously [12] (Table 1). Equivalent amounts of protein were separated by SDS-PAGE and transferred to nitrocellulose filters using the iBlot system (Invitrogen) according to the manufacturer's protocol. Quenched membranes were probed with antibodies and analyzed using the enhanced chemiluminescence reagent Chemi-Lumi One Super (Nacalai Tesque) with an LAS-3000 LuminoImage analyzer (Fujifilm, Tokyo, Japan). Analysis of protein expression levels was performed using the bands obtained from western blotting using Multi Gauge software V3.0 (Fujifilm) as described previously [12].

Immunoprecipitation

Immunoprecipitation was carried out as described previously [8]. Briefly, extracts obtained from patient samples were incubated at 4°C overnight with anti-P5 antibody, and then incubated with Protein G PLUS-Agarose beads for 2 h. After centrifugation for 5 min, the beads were washed three times, and precipitated beads were incubated with loading buffer, and subjected to SDS-PAGE followed by western blotting.

Statistical analysis

Statistical significance at a p-value of less than 0.05 was determined using the Student's t-test.

RESULTS

P5-immunopositive neuronal cells in control brains

We first investigated the immunohistochemical expression of P5 protein in control brain using affinity-purified anti-P5 antibody from rabbit antiserum. In the control specimens, many neurons were immunopositive for the anti-P5 antibody. P5 immunoreactivity was typically observed in the neuronal bodies and dendrites, but nuclei were not stained. The neurons in the frontal lobe were immunostained by the anti-P5 antibody (Fig. 1 A). Anti-P5 antibody-immunopositive neurons were found in the hippocampus and frontal lobe. In addition, many glial cells were also anti-P5 antibody immunopositive (Fig. 1 B).

P5-immunopositive neuronal cells in AD brains

In the tissue sections from patients with AD, we detected numerous P5-immunopositive NFTs (Fig. 1C, D). These P5-immunopositive NFTs were observed in all patients with AD and were found in both the hippocampus and frontal lobe. Other immunoreactivity was not markedly different between the normal and AD brains.

Double staining of P5 and a marker of NFT in AD brains

Immunohistochemical double staining of P5 and AT8 showed that the number of NFTs labeled by antibodies against AT8 was greater than the number of P5-immunopositive NFTs. Anti-P5 and anti-AT8-immunopositive NFTs were co-localized in AD brains (Fig. 2A–C). Quantitative analysis revealed that $78.9 \pm 8.7\%$ of the AT8-immunopositive NFTs were also P5-immunoreactive. The proportions of P5- and AT8-immunopositive NFTs were similar among patients.

Decreased P5 expression in AD brains

Next we investigated the expression levels of PDI and P5 in total protein extracts obtained from control and AD brains. Western blot analysis using anti-P5 antibodies demonstrated that the expression level of P5 in AD brain samples was statistically decreased compared with that of control brain samples, though this was only a trend (Fig. 3A, B; $p = 0.074$). By contrast, the expression level of PDI was not significantly different in the AD brain samples compared with that of control samples. In addition, comparison of the expression levels of P5 and PDI showed that P5 was also decreased in AD brain samples ($p = 0.058$) (Fig. 3B). In agreement with previous findings [15], these results suggest that the expression level of P5 is decreased especially in AD brain whereas the level of PDI is almost unchanged.

S-nitrosylation of P5 in AD brains

We also investigated S-nitrosylation of P5 in AD brain. Total proteins extracted from control and AD brain samples were immunoprecipitated by anti-P5 antibody, and western blot analysis was performed using anti-SNO-Cys. As shown in Fig. 3C, P5 was S-nitrosylated in the brain of two AD patients (cases 2 and 3); however, this was not observed in any control

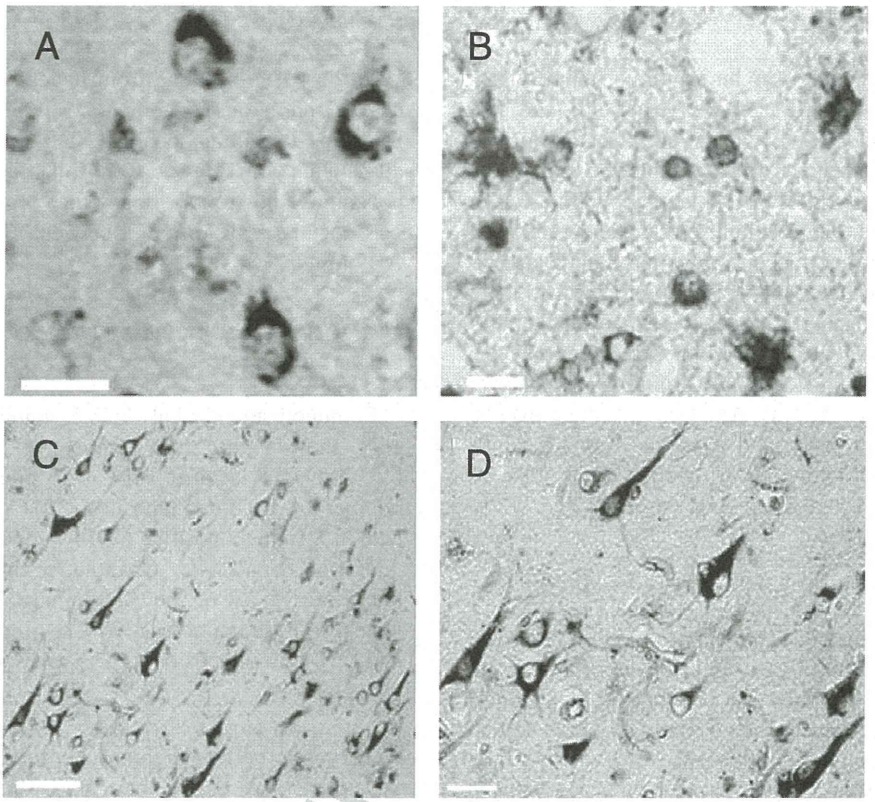

Fig. 1. Immunohistochemical analysis using anti-P5 antibodies. A) Neurons in the frontal lobe of control brain were immunopositive for P5. B) Glial cells were also P5 immunopositive in the frontal lobe of control brain. C, D) Strongly anti-P5-antibody-immunopositive NFTs in the hippocampus of AD brain. Scale bars: A and D = 20 μm, B = 10 μm, C = 50 μm.

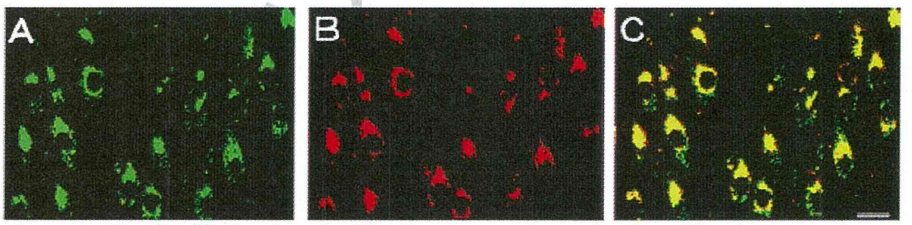

Fig. 2. Double immunostaining of NFTs in the hippocampus of AD brain. A) Anti-P5 antibody immunostaining (green). B) Anti-AT8 antibody immunostaining (red). C) Merge. Scale bar: 20 μm.

brains. It is suggested that the active site cysteine of P5 is also S-nitrosylated in AD brain like PDI.

Knock-down of PDI or P5 decreased the viability of neuronal cells during ER stress

It has been reported that S-nitrosylation inhibited the enzymatic activity of PDI, leading to the accumulation of polyubiquitinated proteins, and activation of the unfolded protein response [9]. In the present study, the expression level of P5 was decreased and S-nitrosylation of P5 was found in AD brain. These results prompted us to investigate the role of P5 in neuronal cell death during ER stress. We confirmed that knock-down of PDI in SH-SY5Y cells by siRNA did not markedly affect the expression level of P5 in the cells, and vice versa (Fig. 4, upper panels), and that these knock-down cells also did not clearly affect the growth of the transfected cells (data not shown). It was found that knock-down of PDI or P5 by siRNA significantly decreased the viability of SH-SY5Y cells under ER stress induced by thapsigargin, which led to the

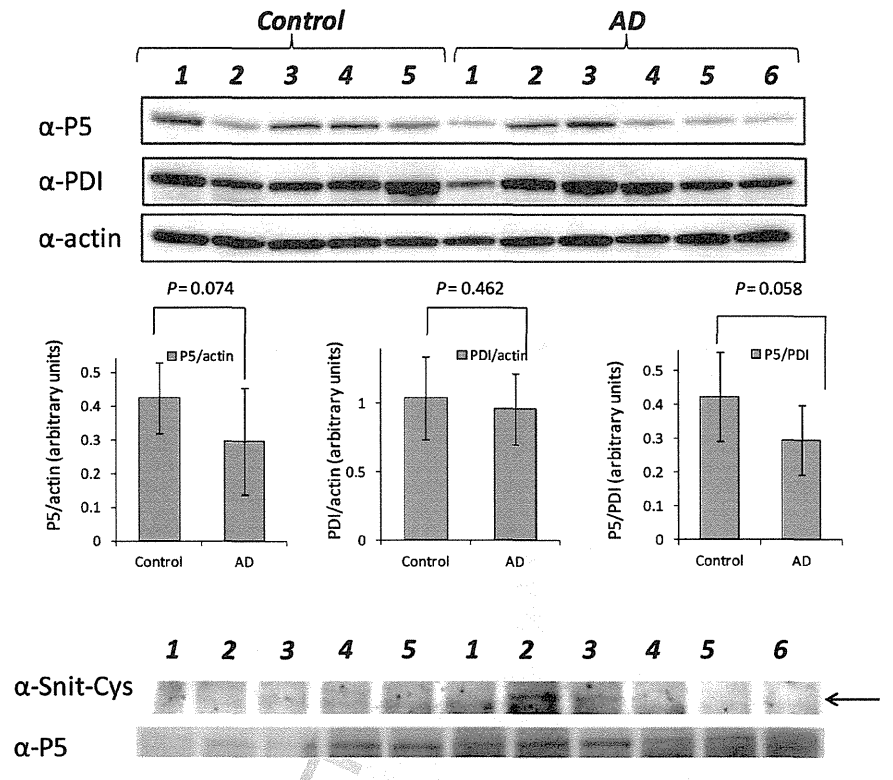

Fig. 3. Western blot analysis of P5 protein in human brain samples. A) Western blotting of PDI and P5 in human brain samples. Protein extracts from six patients with AD and five controls were analyzed by western blotting using anti-PDI and anti-P5 antibodies. β-actin was used as a loading control. Bands were visualized by chemiluminescence as described in the Materials and Methods. B) Expression levels of PDI and P5 in control and AD brain samples. Expression levels were calculated as described in the Materials and Methods. Data represent the mean ± SEM. C) S-nitrosylation of P5 protein in AD brain samples. P5 protein was immunoprecipitated with anti-P5 antibody using extracts obtained from brain samples, and then western blotting was performed using anti-SNO-Cys antibodies as described in the Materials and Methods. Arrow indicates the location of S-nitrosylated P5 protein.

depletion of Ca^{2+} in the ER (Fig. 4, lower graph). It is interesting that over-expression of PDI or P5 by transient transfection with expression vectors had no effect on the viability of SH-SY5Y cells under ER stress (data not shown). These results suggest that the appropriate expression level of P5 is significant for neuronal cell viability especially during ER stress, and these results are correlated with those of western blot analysis using patient samples as discussed above.

DISCUSSION

The ER is a target for endogenously generated reactive oxygen species during aging. It was previously reported that PDI and BiP were oxidatively modified within the livers of elderly mice [16]. Specific activity measurements, performed on purified protein samples obtained from young and old mouse livers, showed definite decreases in BiP ATPase activity and dramatic reductions in PDI enzymatic activity with age. Protein folding and other PDI- and BiP-mediated activities are diminished during aging. Furthermore, the relative loss of these chaperon-like activities could directly contribute to the age-dependent accumulation of misfolded proteins, which is a characteristic of the aging phenotype [16]. As age is the highest risk factor for AD, ER chaperon proteins may be decreased with age, allowing accumulation of misfolded proteins.

Deposition of Aβ is a major pathological hallmark of AD. Recent studies of amyloid-β protein precursor (AβPP) metabolism demonstrated a β/γ-secretase pathway located in the ER that leads to intracellular generation of soluble AβPP and $Aβ_{42}$ peptide [17]. Thus, the ER may be a key site of amyloidogenic AβPP metabolism and AD pathogenesis. Metabolic labeling and immunoprecipitation of transiently transfected human embryonic kidney 293

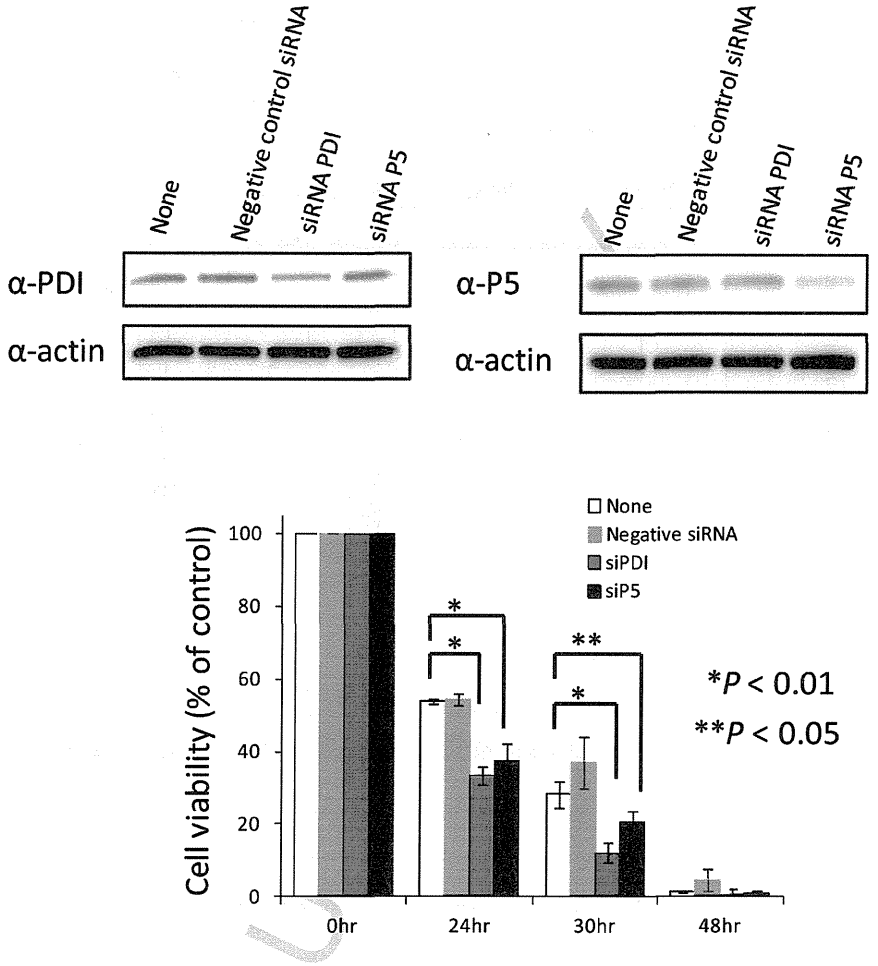

Fig. 4. Effect of knock-down of PDI or P5 on the viability of SH-SY5Y cells under ER stress. Using SH-SY5Y cells, the expression levels of PDI and P5 were confirmed by western blotting 48 h after siRNA transfection (upper panels). β-Actin was used as the loading control. The viability of SH-SY5Y cells after knock-down using siRNA for PDI or P5 with or without induction of ER stress by thapsigargin was assayed as described in the Materials and Methods (lower graph). Cell viability (none, negative siRNA, siPDI, and siP5) without the induction of ER stress at each time (0 h, 24 h, 30 h, and 48 h) was set as a control (i.e., 100%). Data represent the mean ± SD from experiments performed in triplicate. $*p < 0.01$, $**p < 0.05$.

cells demonstrated co-precipitation of AβPP with BiP, revealing their transient interaction in the ER [17]. Maturation of cellular AβPP was impaired by this interaction. It was previously reported that the protein level of BiP was increased in the temporal cortex and hippocampus of AD brain as determined by western blot analysis and, in particular, the protein level of BiP was increased in Braak stages B and C for amyloid deposits [18]. On the other hand, it was also reported that P5 formed a complex with BiP, and that P5 was a specific substrate protein for BiP [19]. In the present study, we found that the protein levels of P5 were decreased in AD (Fig. 3A, B). It has previously been shown that BiP is not co-localized with NFTs in AD brain [11]; however, P5 was co-localized with NFTs in the present study. It is known that PDI prevents neurotoxicity associated with ER stress and protein misfolding, but NO can block the protective effect of the enzyme through S-nitrosylation [9]. This inhibition of PDI leads to ER stress, which can induce apoptosis. It was previously shown that PDI was S-nitrosylated but the level was not increased in AD [9, 15]. In the present study, we confirmed that the protein level of PDI was not up-regulated in AD (Fig. 3A, B). But the protein level of P5 was down-regulated in AD. The expression level may depend on the clinical stages. In addition, we observed S-nitrosylated P5 in two brains from patients with AD, but it was never found in

control brains. As P5 and PDI were S-nitrosylated in AD, S-nitrosylation of members of the PDI family may lead to loss of function. Recently, it was reported that PDI was also S-nitrosylated in amyotrophic lateral sclerosis [20]. Further investigation is needed to determine whether S-nitrosylation of PDI or P5 occurs in other neurodegenerative diseases.

In the present study, we demonstrated the presence of anti-P5 antibody-immunopositive NFTs. Furthermore, AT8-tau and P5 were co-localized in NFTs. To our knowledge, this is the first report of P5-immunopositive inclusion in AD. We assume that NO inhibited P5 and led to the accumulation of unfolded proteins in AD. Abnormally phosphorylated tau or other proteins may accumulate in NFTs and cause ER stress in AD. As P5 acts as a chaperon in neurons, it may bind to tau and become included in NFTs. The co-localization of P5 and tau in NFTs may be linked to the formation of these inclusions. In addition to degeneration of neurons, the cell structure is markedly changed in neurodegenerative disease. The ER is damaged and P5 may come out of the ER. In many destroyed proteins, P5 and tau may be binding strongly and then they are co-localized in NFTs. We also found that knockdown of P5 could decrease the viability of neuronal cells during ER stress induced by thapsigargin, compared with that of control cells. Taken together, these findings suggest that the role of P5 during ER stress is essential for neuronal cell viability, particularly among aging cells.

A limitation of our study is that the samples have serious variation due to the condition after mortal or clinical stages. Thus, we currently speculate that the level of P5 protein would be decreased depending on the clinical stages of AD, and this is one of the most intriguing issues which should make it clearer in our next study.

In summary, we have demonstrated the presence of P5-immunopositive NFTs in AD. Furthermore, we showed that S-nitrosylated P5 was present and the expression level of P5 was decreased in AD brains compared with that of control brains. We speculate that P5 may be increased in early stage due to ER stress. But ER stress was prolonged and then a lot of neuronal cells were destroyed. Finally, P5 may be decreased in advanced stage. In addition, we found that ER stress with P5 dysfunction can cause neuronal cell death. In AD, NO may inhibit P5 by inducing S-nitrosylation, which inhibits its enzymatic activity and thus allows protein misfolding to occur. The accumulation of misfolded proteins induces ER stress, which can cause apoptosis of neuronal cells. These results suggest that P5 could be a therapeutic target to prevent ER stress in neuronal cells in AD.

ACKNOWLEDGMENTS

We thank Mitsuko Tachi, Maiko Yamada, Keiko Shimoura (Department of Pharmacoepidemiology, Kyoto University), and Akiko Yoshida (Department of Neurology, Kyoto University) for excellent technical assistance. This work was in part supported by a research grant from the Alzheimer's Association (IIRG-09-132098) and CREST and Soshinkai Nagaokakyo Hospital.

Authors' disclosures available online (http://www.j-alz.com/disclosures/view.php?id=1889).

SUPPLEMENTARY MATERIAL

Supplementary figures are available in the electronic version of this article: http://dx.doi.org/10.3233/JAD-130632.

REFERENCES

[1] Morishima-Kawashima M, Ihara Y (2002) Alzheimer's disease: Beta-amyloid protein and tau. *J Neurosci Res* **70**, 392-401.

[2] Cras P, Kawai M, Lowery D, Gonzalez-DeWhitt P, Greenberg B, Perry G (1991) Senile plaque neurites in Alzheimer disease accumulate amyloid precursor protein. *Proc Natl Acad Sci U S A* **88**, 7552-7556.

[3] Nakamura T, Lipton SA (2009) Cell death: Protein misfolding and neurodegenerative diseases. *Apoptosis* **14**, 455-468.

[4] Colton CA, Wilcock DM, Wink DA, Davis J, Van Nostrand WE, Vitek MP (2008) The effects of NOS2 gene deletion on mice expressing mutated human AbetaPP. *J Alzheimers Dis* **15**, 571-587.

[5] Kimura T, Horibe T, Sakamoto C, Shitara Y, Fujiwara F, Komiya T, Yamamoto A, Hayano T, Takahashi N, Kikuchi M (2008) Evidence for mitochondrial localization of P5, a member of the protein disulphide isomerase family. *J Biochem* **144**, 187-196.

[6] Noiva R, Lennarz WJ (1992) Protein disulfide isomerase. A multifunctional protein resident in the lumen of the endoplasmic reticulum. *J Biol Chem* **267**, 3553-3556.

[7] Kimura T, Nishida A, Ohara N, Yamagishi D, Horibe T, Kikuchi M (2004) Functional analysis of the CXXC motif using phage antibodies that cross-react with protein disulphide-isomerase family proteins. *Biochem J* **382**, 169-176.

[8] Shitara Y, Tonohora Y, Goto T, YamadaY, Miki T, Makino H, Miwa M, Komiya T (2012) Mitochondrial P5, a member of protein disulphide isomerase family, suppresses oxidative stress-induced cell death. *J Biochem* **152**, 73-85.

[9] Uehara T, Nakamura T, Yao D, Shi ZQ, Gu Z, Ma Y, Masliah E, Nomura Y, Lipton SA (2006) S-nitrosylated protein-disulphide isomerase links protein misfolding to neurodegeneration. *Nature* **441**, 513-517.

[10] Honjo Y, Ito H, Horibe T, Takahashi R, Kawakami K (2010) Protein disulfide isomerase-immunopositive inclusions in patients with Alzheimer disease. *Brain Res* **1349**, 90-96.

[11] Hoozemans JJ, Veerhuis R, Van Haastert ES, Rozemuller JM, Baas F, Eikelenboom P, Scheper W (2005) The unfolded protein response is activated in Alzheimer's disease. *Acta Neuropathol* **110**, 165-172.

[12] Honjo Y, Ito H, Horibe T, Shimada H, Nakanishi A, Mori H, Takahashi R, Kawakami K (2012) Derlin-1-immunopositive inclusions in patients with Alzheimer's disease. *NeuroReport* **23**, 611-615.

[13] Kohno M, Horibe T, Haramoto M, Yano Y, Ohara K, Nakajima O, Matsuzaki K, Kawakami K (2011) A novel hybrid peptide targeting EGFR-expressing cancers. *Eur J Cancer* **47**, 773-783.

[14] Horibe T, Kohno M, Haramoto M, Ohara K, Kawakami K (2011) Designed hybrid TPR peptide targeting Hsp90 as a novel anticancer agent. *J Transl Med* **14**, 8.

[15] Kim HT, Russell RL, Raina AK, Harris PL, Siedlak SL, Zhu X, Petersen RB, Shimohama S, Smith MA, Perry G (2000) Protein disulfide isomerase in Alzheimer disease. *Antioxid Redox Signal* **2**, 485-489.

[16] Nuss JE, Choksi KB, DeFord JH, Papaconstantinou J (2008) Decreased enzyme activities of chaperones PDI and BiP in aged mouse livers. *Biochem Biophys Res Commun* **365**, 355-361.

[17] Yang Y, Turner RS, Gaut JR (1998) The chaperone BiP/GRP78 binds to amyloid precursor protein and decreases Abeta40 and Abeta42 secretion. *J Biol Chem* **273**, 25552-25555.

[18] Hoozemans JJ, Stieler J, van Haastert ES, Veerhuis R, Rozemuller AJ, Baas F, Eikelenboom P, Arendt T, Scheper W (2006) The unfolded protein response affects neuronal cell cycle protein expression: Implications for Alzheimer's disease pathogenesis. *Exp Gerontol* **41**, 380-386.

[19] Jessop CE, Watkins RH, Simmons JJ, Tasab M, Bulleid NJ (2009) Protein disulphide isomerase family members show distinct substrate specificity: P5 is targeted to BiP client proteins. *J Cell Sci* **122**, 4287-4295.

[20] Walker AK, Farg MA, Bye CR, McLean CA, Horne MK, Atkin JD (2010) Protein disulphide isomerase protects against protein aggregation and is S-nitrosylated in amyotrophic lateral sclerosis. *Brain* **133**, 105-116.

Acta Neuropathol (2014) 127:685–698
DOI 10.1007/s00401-014-1259-1

ORIGINAL PAPER

Neurofibrillary tangle formation by introducing wild-type human tau into APP transgenic mice

Tomohiro Umeda · Satomi Maekawa · Tetsuya Kimura · Akihiko Takashima · Takami Tomiyama · Hiroshi Mori

Received: 24 August 2013 / Revised: 6 February 2014 / Accepted: 6 February 2014 / Published online: 15 February 2014

Abstract Senile plaques comprised of Aβ aggregates and neurofibrillary tangles (NFTs) composed of hyperphosphorylated tau filaments are the hallmarks of Alzheimer's disease (AD). A number of amyloid precursor protein (APP) transgenic (Tg) mice harboring APP mutations have been generated as animal models of AD. These mice successfully display amyloid plaque formation and subsequent tau hyperphosphorylation, but seldom induce NFT formations. We have demonstrated that the APP_{OSK}-Tg mice, which possess the E693Δ (Osaka) mutation in APP and thereby accumulate Aβ oligomers without plaques, exhibit tau hyperphosphorylation at 8 months, but not NFT formation even at 24 months. We assumed that APP-Tg mice, including ours, failed to form NFTs because NFT formation requires human tau. To test this hypothesis, we crossbred APP_{OSK}-Tg mice with tau-Tg mice (tau264), which express low levels of 3-repeat and 4-repeat wild-type human tau without any pathology. The resultant double Tg mice displayed tau hyperphosphorylation at 6 months and NFT formation at 18 months in the absence of tau mutations. Importantly, these NFTs contained both 3-repeat and 4-repeat human tau, similar to those in AD. Furthermore, the double Tg mice exhibited Aβ oligomer accumulation, synapse loss, and memory impairment at 6 months and neuronal loss at 18 months, all of which appeared earlier than in the parent APP_{OSK}-Tg mice. These results suggest that Aβ and human tau synergistically interact to accelerate each other's pathology, that the presence of human tau is critical for NFT formation, and that Aβ oligomers can induce NFTs in the absence of amyloid plaques.

Keywords Aβ oligomers · Tau filaments · Synapse loss · Neuronal loss · Alzheimer's disease

Introduction

Senile plaques comprised of Aβ fibrils and neurofibrillary tangles (NFTs) composed of hyperphosphorylated tau filaments are the hallmarks of Alzheimer's disease (AD). It was believed that Aβ deposition triggers abnormal phosphorylation of tau, which leads to NFT formation and neurodegeneration [17]. Based on this hypothesis, a number of amyloid precursor protein (APP) transgenic (Tg) mice have been generated as animal models of AD. By introducing one or more APP mutations identified in familial AD into the transgene, these mice successfully displayed amyloid plaque formation and subsequent tau hyperphosphorylation within neurons surrounding the plaques, but seldom induced NFT formations [12]. Several groups have established mouse models of AD showing both amyloid plaques and NFTs by crossbreeding mutant APP-Tg mice with mutant tau-Tg mice [4, 18, 26, 35, 37, 38, 41]. However, these models do not exactly reflect the pathogenesis of AD,

Electronic supplementary material The online version of this article (doi:10.1007/s00401-014-1259-1) contains supplementary material, which is available to authorized users.

T. Umeda · S. Maekawa · T. Tomiyama (✉) · H. Mori
Department of Neuroscience, Osaka City University Graduate School of Medicine, 1-4-3 Asahimachi, Abeno-ku, Osaka 545-8585, Japan
e-mail: tomi@med.osaka-cu.ac.jp

T. Umeda · T. Tomiyama · H. Mori
Core Research for Evolutional Science and Technology, Japan Science and Technology Agency, Kawaguchi, Japan

T. Kimura · A. Takashima
Department of Aging Neurobiology, Center for Development of Advanced Medicine for Dementia, National Center for Geriatrics and Gerontology, Obu, Japan

since no mutations in tau have been found in AD and since tau mutations themselves can cause NFT formation in mice independent of Aβ deposition [14].

Recent evidence suggests that Aβ oligomers, rather than Aβ fibrils, are the causal molecule in AD [23]. In cultured rat primary neurons, exogenously added Aβ oligomers induced tau hyperphosphorylation and neurodegeneration [11, 21]. We have shown that the E693Δ (Osaka) mutation in APP, which was found in Japanese pedigrees with familial AD, causes disease by enhancing Aβ oligomerization without amyloid plaque formation [47]. We generated APP-Tg mice harboring this mutation (APP_{OSK}-Tg mice) to study the pathological roles of Aβ oligomers in AD in vivo [46]. The levels of expression of human APP in the mice were almost the same as those of endogenous mouse APP. The APP_{OSK}-Tg mice showed intraneuronal accumulation of Aβ oligomers, synapse loss, and memory impairment at 8 months and eventual neuronal loss at 24 months. Tau hyperphosphorylation also occurred at 8 months, but NFT formation did not even at 24 months. We assumed that APP-Tg mice, including ours, failed to form NFTs because these mice lacked certain factors necessary for NFT formation.

The formation of NFTs in old age has been reported to occur not only in humans but also in other species, including chimpanzees [39], baboons [40], cynomolgus monkeys [36], cheetahs [42], and cats [6]. On the other hand, mice and rats are known not to form NFTs. We compared the amino acid sequences of tau across humans, chimpanzees, cats, and mice, which are available from the NCBI database. We found apparent differences in amino acid sequence between human and mouse tau, particularly in the N-terminal regions. In contrast, chimpanzee tau is almost identical to human tau and cat tau shows higher structural homology with human tau than with mouse tau. These observations led us to hypothesize that NFT formation requires certain sequences which exist in human tau but not in mouse tau.

To elucidate this possibility, here we generated double Tg mice by crossbreeding APP_{OSK}-Tg mice with our wild-type human tau-Tg mice. The tau-Tg mice, originally referred to as line 264 and hereafter termed tau264, were designed to express both 3-repeat (3R) and 4-repeat (4R) human tau at a comparable ratio to that in adult human by inserting tau intronic sequences into both sides of tau exon 10 in the transgene [48]. The levels of expression of human tau in tau264 mice were only 10 % those of endogenous mouse tau, and no pathological changes were observed even at 24 months. The resultant double Tg mice displayed tau hyperphosphorylation at 6 months and NFT formation at 18 months in the absence of tau mutations. Importantly, these NFTs contained both 3R and 4R human tau, similar to those in AD [15]. Furthermore, double Tg mice exhibited intraneuronal accumulation of Aβ oligomers, synapse loss, and memory impairment at 6 months and neuronal loss at 18 months, all of which appeared earlier than in the parent APP_{OSK}-Tg mice. These results suggest that Aβ and human tau synergistically interact to accelerate each other's pathology and that the presence of human tau is critical for Aβ-induced NFT formation. Our findings also indicate that Aβ oligomers can induce NFTs in the absence of amyloid plaques.

Materials and methods

Generation of double Tg mice

Heterozygotes of the APP_{OSK}-Tg mice [46], which express human APP695 with the Osaka mutation under the mouse prion promoter, were mated with heterozygotes of the tau264 mice [48], which express 3R and 4R wild-type human tau by the presence of tau intronic sequences under the mouse calcium/calmodulin-dependent kinase IIα promoter. The siblings were examined for their genotype by genome PCR and were accordingly divided into four groups: non-Tg, APP_{OSK}-Tg, tau264, and double Tg expressing both APP_{OSK} and wild-type human tau. The single and double Tg mice were heterozygous for each transgene of interest and have the same genetic background as C57BL/6 mice. All animal experiments were approved by the ethics committee of Osaka City University (Osaka, Japan) and were performed in accordance with the Guide for Animal Experimentation, Osaka City University. Every effort was made to minimize the number of animals used and their suffering.

Antibodies

Rabbit polyclonal antibodies reactive to both human and mouse tau (pool-2) [45], specific to 4R tau (R2) [45], and reactive to both human and mouse Aβ (β001) [28] were prepared in our laboratory. The mouse monoclonal antibody to pSer396/Ser404-tau (PHF-1) was a kind gift from Dr. Peter Davies (Department of Pathology, Albert Einstein College of Medicine, Bronx, NY). Mouse monoclonal antibodies specific to human APP (6E10; Covance, Princeton, NJ), Aβ oligomers (11A1; IBL, Fujioka, Japan), human tau (tau12; Abcam, Cambridge, UK), 3R tau (RD3; Merck Millipore, Billerica, MA), 4R tau (RD4; Merck Millipore), pSer202/Thr205-tau (AT8; Thermo Scientific, Waltham, MA), synaptophysin (SVP-38; Sigma, St. Louis, MO), the mature neuron marker NeuN (Chemicon, Temecula, CA), and rabbit antibodies specific to the postsynaptic density protein PSD-95 (Cell Signaling Technology, Danvers, MA) and actin (Sigma) were purchased.

Western blot

Mouse brains (n = 4 for each group) were homogenized by sonication in 4 volumes of 50 mM Tris–HCl, pH 7.6, 150 mM NaCl (TBS) containing protease inhibitor cocktail (P8340; Sigma). The homogenates were subjected to SDS-PAGE with 7 % NuPage Tris–Acetate gels (Invitrogen, Carlsbad, CA) and transferred to PVDF membranes (Millipore). APP, tau, and actin were probed with 6E10, tau12, and anti-actin antibodies followed by HRP-labeled second antibodies and the chemiluminescent substrate Immobilon Western (Millipore). Signals were visualized and quantified using a LAS-3000 luminescent image analyzer (Fujifilm, Tokyo, Japan).

The homogenates (n = 3–4 for each group) were fractionated by three-step ultracentrifugation including TBS, *N*-lauroylsarcosinate (sarkosyl), and guanidine hydrochloride (GuHCl) extraction, as described previously [48]. The GuHCl-extracts were 400-fold diluted in TBS containing P8340 and concentrated into the initial volumes using Amicon Ultra 30 K filter devices (Millipore). The 30 K flow-through fractions were pooled for detection of low-n Aβ oligomers (see below). Phosphorylated tau in the TBS- and neutralized GuHCl-extracts was detected by Western blot with PHF-1 and AT8 antibodies. Aliquots of the TBS- and neutralized GuHCl-extracts were treated with 400 U/ml (approximately 80 U/mg protein) of calf intestinal alkaline phosphatase (New England Biolabs, Ipswich, MA) at 37 °C overnight, as described previously [48]. Dephosphorylated tau in the treated samples was probed with tau12, RD3 and RD4 antibodies.

For detection of Aβ oligomers higher than 30 kDa, the TBS- and neutralized GuHCl-extracts were applied onto 7 % Tris–Acetate gels, transferred to PVDF membranes, and stained with β001 antibody after the membranes were boiled in PBS for 10 min. To detect low-n Aβ oligomers, Aβ in the TBS-extracts and the 30 K flow-through fractions of GuHCl-extracts were immunoprecipitated with 6E10

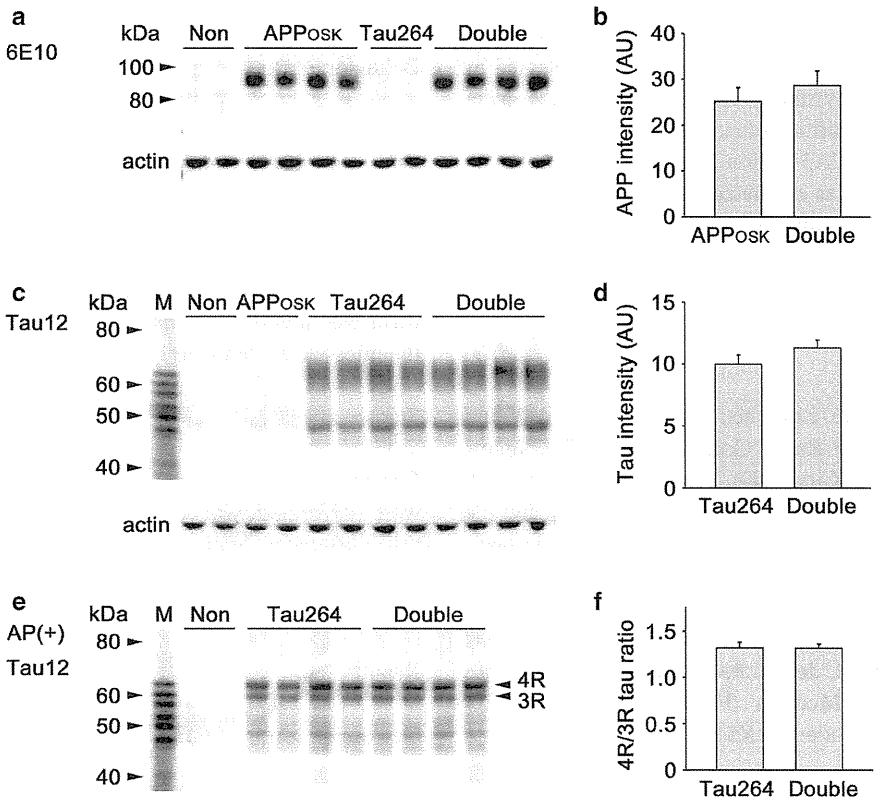

Fig. 1 Expression levels of human APP and tau in double Tg mice. **a** Brain homogenates from 6-month-old mice were subjected to Western blot with human APP-specific 6E10 antibody and anti-actin antibody. *Non* non-Tg mice, *Double* double Tg mice. **b** No significant difference in the expression level of human APP was observed between parent APP_{OSK}-Tg mice and double Tg mice. *AU* arbitrary unit. **c** Brain homogenates from 6-month-old mice were subjected to Western blot with human tau-specific tau12 antibody and anti-actin antibody. *M* recombinant human tau 6 isoforms. **d** No significant difference in the expression level of human tau was observed between parent tau264 mice and double Tg mice. **e** TBS-extracts from the brains of 6-month-old mice were treated with alkaline phosphatase (AP) and subjected to Western blot with tau12 antibody. **f** No significant difference in the ratio of 4R/3R tau was observed between parent tau264 mice and double Tg mice

antibody, applied onto 12 % NuPage Bis–Tris gels, and stained with β001 antibody after boiling the membranes.

Immunohistochemistry and Gallyas silver staining

Mice ($n = 4$–6 for each group) were perfused with 4 % paraformaldehyde, and the brains were removed, embedded in paraffin, and sectioned at 5 μm. Aβ accumulation and tau phosphorylation at 4, 6, 8, 12, 18, and 24 months, synapse loss at 6 and 12 months, and neuronal loss at 18 and 24 months were examined by immunohistochemistry, as described previously [46, 48]. Tangle formation was examined by Gallyas silver staining at 12, 18, and 24 months, as described previously [48]. The co-localization of 3R and 4R tau in cytoplasmic inclusions was examined at 24 months by double immunostaining with R2 and RD3 antibodies followed by FITC- and rhodamine-labeled second antibodies. Specimens were observed under a BX50 microscope (Olympus, Tokyo, Japan) and a Leica TCS SP5 confocal laser microscope (Leica, Wetzlar, Germany). Aβ oligomer accumulation was evaluated at 6 and 12 months by quantifying 11A1-positive areas in each photograph using NIH ImageJ software. Synapse loss was assessed by quantifying synaptophysin and PSD-95 fluorescence intensities in the apical dendritic-somata field (30 μm × 60 μm) of the hippocampal CA3 region using NIH ImageJ software. Neuronal loss was estimated by counting NeuN-positive cells in an area within 800 μm along the pyramidal cell layer of the hippocampal CA3 region and in an area of 1 × 1 mm in the retrosplenial region of the cerebral cortex.

Golgi staining

Dendritic spines were examined at 6 months by Golgi staining using the FD Rapid GolgiStain Kit (FD Neurotechnologies, Ellicott City, MD). Mice ($n = 1$–2 for each group) were perfused with 4 % paraformaldehyde, and the brains were removed and processed according to the manufacturer's instructions. After impregnation, brains were cut into 100 μm sections using a cryostat at −20 °C and mounted on gelatin-coated microscope slides. The sections were air-dried, stained, dehydrated, and coverslipped with Permount Mounting Medium (Fisher Scientific). Specimens were observed under a BX51 microscope (Olympus).

Immunoelectron microscopy

Tau filament formation was examined by post-embedding immunoelectron microscopy at 12, 18, and 24 months, as described previously [48]. Mouse brains ($n = 1$–2 for each group) were fixed in 4 % paraformaldehyde, 2.5 % glutaraldehyde, then 1 % osmium tetroxide, and embedded in epoxy resin. 70 nm-thick ultrathin sections were prepared and placed on H75-mesh carbon-coated copper grids. The sections were blocked with 5 % BSA/PBS and incubated with pool-2 antibody followed by 10 nm gold particle-labeled second antibody (AuroProbe EM GAR G10; Amersham). The specimens were then stained with 2.5 % lead citrate and 5 % uranyl acetate and viewed under an H-7500 electron microscope (Hitachi High-Technologies, Tokyo, Japan).

Fig. 2 Accelerated accumulation of intraneuronal Aβ oligomers in double Tg mice. **a** Brain sections were stained with Aβ oligomer-specific 11A1 antibody at various ages. APP_{OSK}-Tg mice exhibited intraneuronal accumulation of Aβ oligomers in the hippocampal CA3 region, cerebral cortex (CTX), and to a lesser extent the hippocampal CA1 region at 8 months. Double Tg mice displayed intraneuronal accumulation of Aβ oligomers in the CA3 region, cerebral cortex, and to a lesser extent the CA1 region at 6 months, which is earlier than parent APP_{OSK}-Tg mice. *Scale bar* 30 μm. **b** 11A1-positive areas in each photograph were quantified at 6 and 12 months using NIH ImageJ software. Data are given as mean ± SEM ($n = 5$ for non-Tg and APP_{OSK}-Tg at 6 months, $n = 4$ for tau264 and double Tg at 6 months, $n = 5$ for non-Tg, APP_{OSK}-Tg and tau264 at 12 months, $n = 4$ for double Tg at 12 months)

Behavioral tests

Spatial reference memory in mice was assessed at 6 months using the Morris water maze, essentially as described previously [46]. Male mice ($n = 5$–10 for each group) were trained to swim to a hidden platform for five consecutive days. Training consisted of five trials per day with intertrial intervals of 5 min, and the time required to reach the platform was measured in each trial. Locomotor activities of the mice were examined by an open-field test [46].

Statistical analysis

Comparisons of means among more than two groups were performed with ANOVA followed by Fisher's PLSD test. Differences with a p value of <0.05 were considered significant.

Results

Expression levels of human APP and tau in double Tg mice

To investigate the role of human tau in NFT formation, we crossbred APP_{OSK}-Tg mice with tau264 mice. The siblings were divided into four groups according to their genotype: non-Tg, APP_{OSK}-Tg, tau264, and double Tg, which express both APP_{OSK} and wild-type human tau. The levels of expression of APP and tau were examined by Western blot with human APP-specific 6E10 antibody and human tau-specific tau12 antibody at 6 months. No significant differences

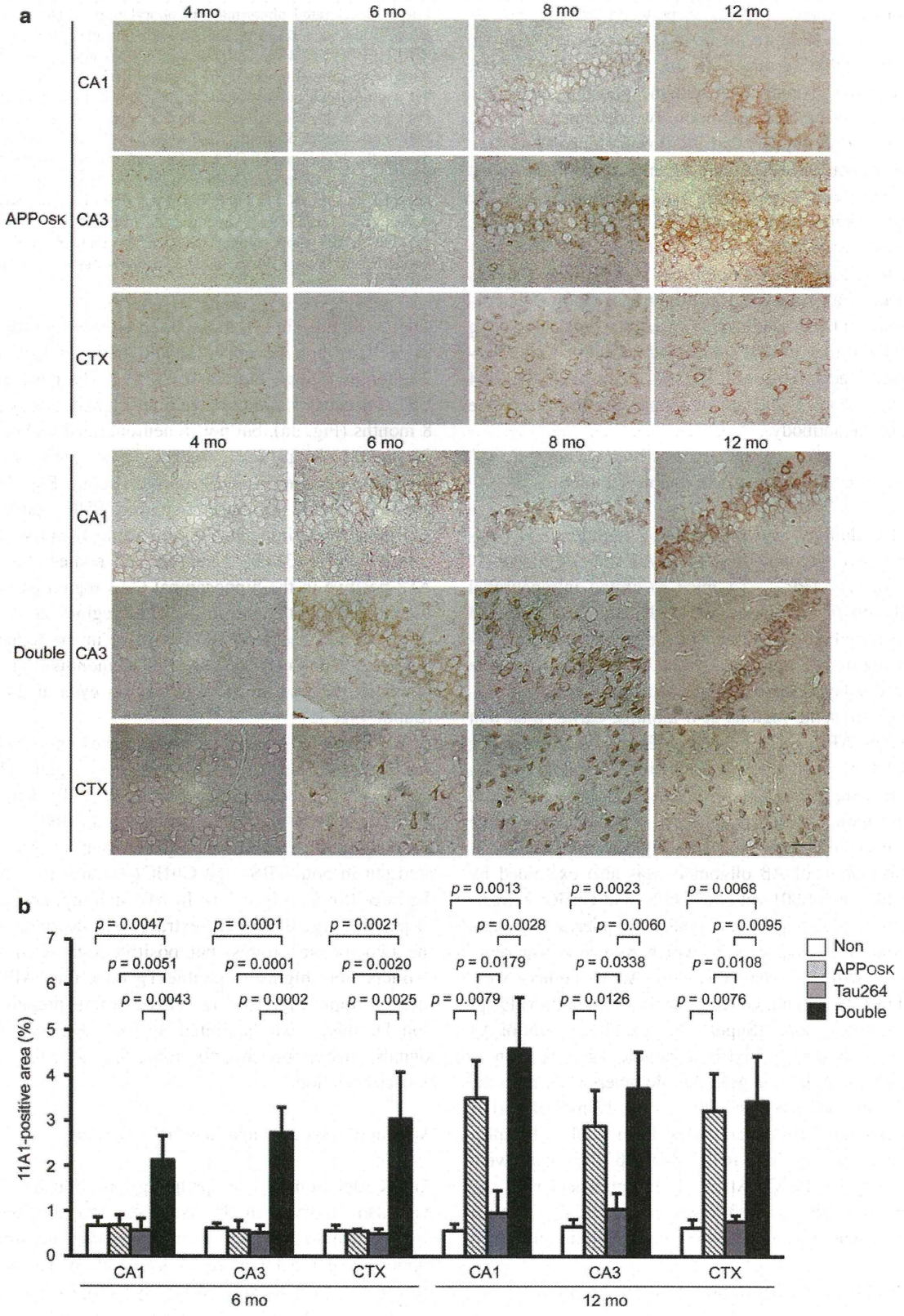
a
4 mo
6 mo
8 mo
12 mo
APPosk
CA1
CA3
CTX
Double
b
11A1-positive area (%)
p = 0.0047
p = 0.0051
p = 0.0043
p = 0.0001
p = 0.0001
p = 0.0002
p = 0.0021
p = 0.0020
p = 0.0025
p = 0.0013
p = 0.0028
p = 0.0179
p = 0.0079
p = 0.0023
p = 0.0060
p = 0.0338
p = 0.0126
p = 0.0068
p = 0.0095
p = 0.0108
p = 0.0076
Non
APPosk
Tau264
Double
6 mo
12 mo